IEEE Access
Multidisciplinary ⋮ Rapid Review ⋮ Open Access Journal

Received September 2, 2020, accepted September 13, 2020, date of publication September 18, 2020,
date of current version October 5, 2020.

Digital Object Identifier 10.1109/ACCESS.2020.3024556

Zonal Thermal Room Original Model With Kron's Method

RIVO RANDRIATSIFERANA[1], (Member, IEEE), LALA RAJAOARISOA[2], SAMUEL NGOHO[3], WENCESLAS RAHAJANDRAIBE[4], (Member, IEEE), AND BLAISE RAVELO[5], (Member, IEEE)

[1]LE2P Lab, University of La Reunion, 97744 Saint Denis, France
[2]Unité de Recherche en Informatique et Automatique, IMT Lille Douai, University of Lille, 59000 Lille, France
[3]Association Française de Science des Systèmes (AFSCET), 75000 Paris, France
[4]IM2NP, CNRS, UMR 7334, Aix-Marseille University, University of Toulon, 13007 Marseille, France
[5]School of Electronic and Information Engineering, Nanjing University of Information Science and Technology (NUIST), Nanjing 210044, China

Corresponding author: Samuel Ngoho (samngoho@yahoo.fr)

This work was supported by the European project "SHINE: Sustainable Houses in Inclusive Neighborhoods". The project is granted by Interreg 2 Seas and the European Regional Development Fund. The authors address also a grateful thank to Dr. Olivier Maurice from Ariane Group, Mureaux, France for his scientific help to construct the Kron's model.

ABSTRACT An original thermal model of a single room structure is developed by using the tensorial network-based Kron's method. The modelling principle is using the equivalent RC-network of wall, door and air constituting the house. For a better understanding, the temperature propagation was assumed only in a 1-D horizontal direction. The problem geometrization is defined in function of rectangular approximation meshing. After the determination of the equivalent thermal resistor and thermal capacitor, the innovative thermal circuit representing the room is elaborated. The methodology of the Kron's formalism, implicitly described with the different action steps is introduced. The thermal room Kron's method is implemented from the branch to mesh spaces before the expression of the problem metric. The thermal transfer functions (TTFs) at three cases of indoor points, situated near, middle and far of the door are established from the Kron's problem metric. The feasibility of the room thermal Kron's TTF model is validated with SPICE TTF simulations in both frequency and time domains. The thermal cut-off frequencies are verified with very good correlation between the established TTF model and simulation. An excellent prediction of transient responses with unit-step and arbitrary waveform temperature signals with a minimal and maximal amplitude of about 20°C and 40°C is proposed.

INDEX TERMS Thermal modelling, room model, zonal model, RC-network, 1-D propagation, Kron's method, frequency domain analysis, transient response, thermal transfer function (TTF).

I. INTRODUCTION

The modern urban city design engineering should overcome the energy and thermal comfort performances [1], [2]. The building engineers are wondering constantly about the ideal room temperature for the comfort living [3].

To face up this challenge, an efficient investigation must be conducted on the dependence between the indoor and outdoor temperature in function of the climate environment [4]. Diverse solutions were deployed against the building and home comfort performances [5]–[8]. Innovative smart home technology was introduced in order to adapt the indoor and outdoor temperatures [5]. Material and architectural solutions based on the insulating layer location, distribution and orientations were developed [6],[7]. Seasonal passive design strategies were also introduced [8]. Whatever the envisaged solutions, an efficient predictive approach is undeniably helpful for the building engineers during the design phases.

Emphatically, thanks to the tremendous boom of the computer-aided design, simulation tools [9]–[14] were developed. The trends of the simulation were aimed to the multiple objectives as the numerical method order reduction [10], building energy efficiency [11], distributed computation technique [12], novel approach to overcome legacy code limitations [13], [14] and the sensitivity of peak-load reduction computing tool in the function of environmental

The associate editor coordinating the review of this manuscript and approving it for publication was Wen-Sheng Zhao.

preference [15]. Substantially, the popular development of thermal building computation tool depends on the numerical methods of the solver algorithm. Different mathematical approaches were investigated in function of the building structure. Preliminarily, stochastic differential equation-based modelling was introduced to calculate the heated dynamic through the building [16]. However, the differential equations can be analytically complex to manipulate according to the building geometrical structure and geometrical parameters. Therefore, a more practical grey box approach with a minimum number of geometrical parameters was introduced [17]. But the pragmatic control of grey box model depends on the thermal structure representation. To improve the performances, numerical model reduction of the thermal building with innovative strategies as an aggregation of states was introduced [18], [19]. But more efficient model allowing to understand the temperature propagation through the different layers of the building seems to be a more rigorous solution.

The adequate solution with the best efficiency seems to be the model inspired by the electrical circuit analogy [20]. Such an approach was described as a thermal network model [20]–[27]. Of course, the thermal network requires an accurate approximation of thermal resistors and thermal capacitors representing each element constituting the building [21], [22]. A low order thermal network for dynamic state of buildings on the city district scale was proposed in [23]. The thermal network model was proposed with the possibility to assess the building energy efficiency [24]. Despite the different deployments of the thermal network modelling, few approaches are available in the literature for the assessment of the temperature through each thermal components of the thermal circuit. One of the prominent methods allowing to overcome this technical limitation is based on the unfamiliar tensorial analysis of networks (TAN) using Kron's method [25]. The feasibility of the TAN thermal building modelling for calculating the multiwall thermal transfer function (TTF) was initiated in [25]. However, the case of more general configuration with a room configuration remains an open question from the thermal building engineers. The main purpose of the present paper is to answer to such a scientific curious question, by focusing on the original modelling of thermal room. Before reaching the main study, it is worth to start with a brief bibliographical word on the unfamiliar Kron's method.

The Kron's method was initiated in the 1930s for the treatment of electrical machine structures [27]. This unfamiliar method is intended to analyze electrical networks based on the tensorial representation in different spaces as branch, nodes, summits, meshes, moments, etc. The unfamiliar Kron's method offers a powerful abstraction of electrical engineering systems and networks. The power of the modelling abstraction has been revealed, since the 1990s, by Maurice and his team, with the capacity of Kron's method to analyze complex electromagnetic compatibility systems [28], [29]. Moreover, the Kron's method was also used to calculate fastly multi-port electrical circuits with the flexibility between impedance, admittance and S-matrix representations [30]. A preliminary study on the electrothermal modelling of an electronic component with the Kron's method is initiated in [31]. Despite, research work performed on the Kron's method modelling of electronic and electrical circuits [27]–[30], the method is not at all familiar to the thermal research engineer. For this reason, an original thermal network modelling of room indoor temperatures is explored in this work. The developed modeling approach will provide an overview on how we can manage building thermal flows in a general manner according to the Kron's formalism. The knowledge about the thermal performance is useful to design and control heating and cooling systems in the building environment. Moreover, as the Kron's method guarantees a literally fast computation time, the developed model can be exploited in the future to predict quickly the performances of building in function of materials and geometry. But a simple case of study should be performed to illustrate the developed model understandability and feasibility.

The present paper is organized in four main sections described as follows:

- Section II is dedicated to the room structure problem formulation. The 3-D representation of the room will be described. Then, the basic way to determine the equivalent building block elements as the thermal resistors and thermal capacitors will be introduced.
- Section III is focused on the main action about the Kron's method modelling of the building thermal network. First, the classical thermal circuit will be defined. Then, the thermal structure equivalent graph topology will be explored. The branch and mesh space analyses will be drawn in order to determine the TTF at the different meshing indoor test points.
- Section IV introduces the validation of the thermal Kron's model. First, the proof-of-concept (POC) of a room structure will be parametrized and then, the comparisons between the calculated and simulated TTF will be discussed. The performance of the developed method will be pointed out with respect to the existing thermal simulators [32].
- Then, Section V is the final conclusion.

II. STATEMENT OF THE ROOM THERMAL MODEL PROBLEM

The present section formulates the thermal room problem under investigation. The problem statement must begin with the consideration of the room structure 3-D description. After that, we will introduce the elaboration of the equivalent thermal resistor and thermal capacitor constituting each element of the room.

A. 3-D DESCRIPTION OF THE ROOM UNDER INVESTIGATION

In the present study, we consider a computer server room which is located in the basement of the building. The location

is well-isolated over the three sides, except the front face, as illustrated in Fig. 1(a). In fact, the main goal of the present modelling is to evaluate the different internal temperatures. In mid-term, according to the requirement about the comfort temperature for the future building standard, the proposed model may serve to choose the optimal place, where we can install the fan and optimize its control, under fast computation.

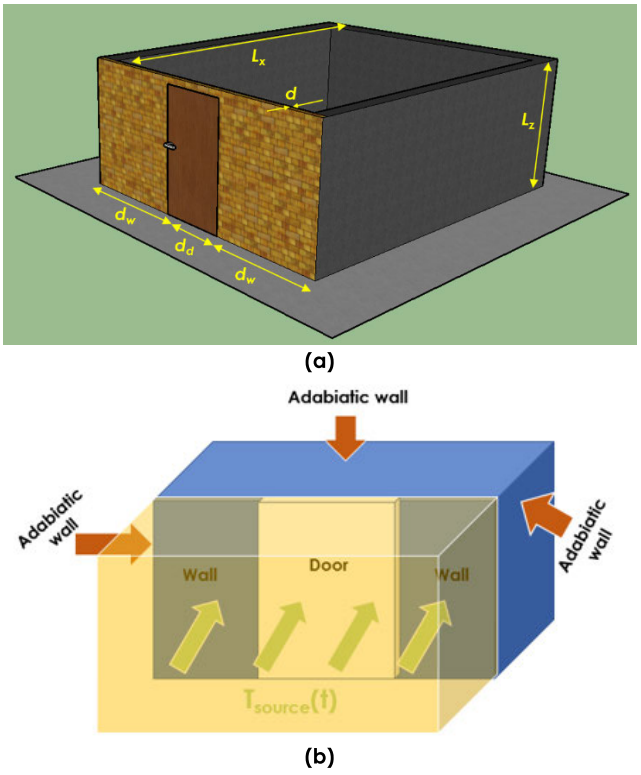

FIGURE 1. 3-D configuration of the room under study.

For the better understanding and the feasibility study, Fig. 1(a) shows the 3-D configuration of the room assumed as a rectangular box with geometrical size, $(L_x \times L_y \times L_z)$. The pieces of lateral wall and the door in the face exposed to the heat temperatures present widths, d_w and d_d, respectively. That is why, the room physical length was set equal to $L_y = 2d_w + d_d$. For the sake of understanding of the proposed modelling method mechanism, in the present study, we assume the following hypotheses.

Under such conditions, the circumstance of the scenario is assumed integrating the climate environment and thermodynamic law's:

- The structure is supposed influenced by an outdoor temperature, $T_{out} = T_{source}$, higher than the indoor temperature.
- The temperature is propagating inward along the one horizontal direction.
- The temperature is constant in vertical direction. Transitively, the problem can be reduced as 2-D representation through any horizontal cut-plane.
- The outdoor side is assumed separated by the wall side with the door.
- The environment humidity, wind effect and indoor shadow are neglected.
- And the other three sides of the room are assumed to be adiabatic as explained in Fig. 1(b). In other words, these faces are assumed to be in the ideal case of well isolated from the other adjacent rooms.

B. POSITIONNING OF THE INDOOR NODES FOR THE UNKOWN TEMPERATURES

Before the elaboration of the equivalent thermal network of the room, it would be necessary to define the key points where the temperature needs to be assessed. To do this, different nodes are taken as reference test points in the room. Fig. 2 highlights the positioning configuration of the indoor test nodes. The meshing strategy can be determined based on the inhomogeneity of the facing wall and the indoor nodes positioning according to the distance with the door. Subsequently, our main interest in the present study can be formulated by the determination of:

- Near test plane which corresponds to the temperature near the door or in the internal face of the wall,
- Middle test plane which designates the temperature in the medium line of the room,
- And far test plane is the temperature at the nodes in the opposite side of the door and back of the room.

After this geometrical analysis, let us describe the systemic approach of the room thermal modelling.

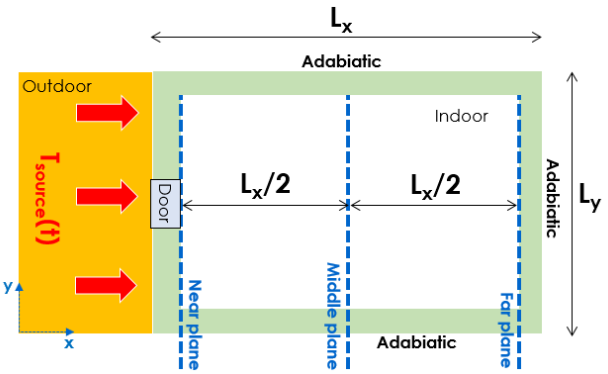

FIGURE 2. Top view of the room structure showing the node positioning.

C. SYSTEM APPROACH OF THE THERMAL MODELLING PROBLEM

To model the indoor temperature of the room, we will proceed with systemic approach as explored in [20]–[27]. The present subsection introduces the representative thermal model of the room structure.

1) RECALL ON THE SYSTEMIC BLACK BOX MODEL

Fig. 3 represents the general diagram of the thermal black box for treating the thermal problem. It acts as a two-port

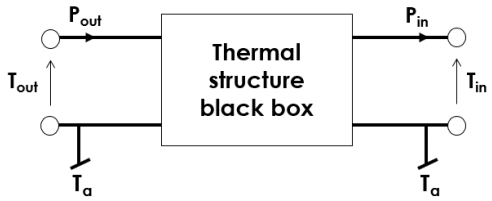

FIGURE 3. General representation of thermal structure black box.

system under the reference temperature of the ambient environment denoted T_a. The excitation source is represented by temperature, T_{out}, and the unknown indoor temperature is denoted T_{in}. The power flux of each port is denoted by P_{out} and P_{in}, respectively.

Under the symbolic Laplace variable, s, the analytical TTF model associated to the thermal system is defined by:

$$TTF(s) = \frac{T_{in}(s)}{T_{out}(s)}. \tag{1}$$

Similar to the frequency responses familiarly exploited for the electrical system analyses [28]–[30], the associated magnitude and phase of the proposed TTF can be written as respectively:

$$TTF_{dB}(\omega) = 20 \log |TTF(j\omega)| \tag{2}$$

$$\varphi(\omega) = \arg [TTF(j\omega)]. \tag{3}$$

the angular frequency complex variable, $s = j\omega$.

2) ANALYTICAL DEFINITION OF THERMAL RESISTOR AND CAPACITOR

The basic structure corresponding to the thermal elementary components is presented essentially as parallelepiped homogenous material as explained in Fig. 4. In this case, this rectangular 3-D bulk element is described with physical dimensions ($s_1 \times s_2 \times s_3$).

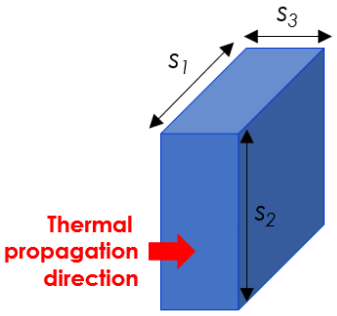

FIGURE 4. Homogenous bulk of parallelepiped element.

The following thermal resistor and capacitor are defined under the thermal propagation direction indicated in Fig. 4. By denoting the bulk material thermal conductivity, λ, the associated thermal resistor is analytically defined by [33]:

$$R = \frac{s_3}{\lambda\, s_1\, s_2}. \tag{4}$$

By denoting the bulk material specific heat, h, and mass density, ρ, the thermal capacitor is analytically defined by [33]:

$$C = \rho\, h\, s_1\, s_2\, s_3. \tag{5}$$

Knowing these R and C parameters, the RC thermal networks can be drawn in function of the structure as the case of the room scenario given in Fig. 2.

3) RC-NETWORK EQUIVALENT TO THE ELEMENTARY STRUCTURE

The common way to treat such a structure depends on the fundamental network of each elementary block constituting the system. The building block of the thermal RC network modelling is shown in Fig. 5(a). This illustrative elementary bulk structure consists of outdoor air-wall material-indoor air by supposing that the temperature is propagating from outdoor to indoor in 1-D direction. The reference nodes, M_{out} and M_{in} enable to define the equivalent network. This structure can be modelled as the content of the black box introduced in Fig. 3(a) with its thermal resistance, R, and thermal capacitor, C, [20]–[27] interconnected as depicted in Fig. 5(b).

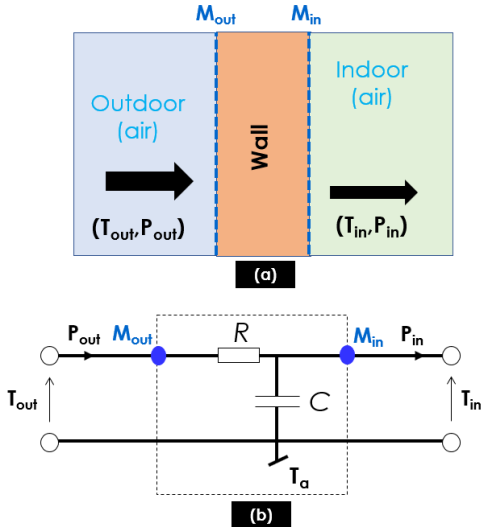

FIGURE 5. (a) Outdoor air-wall-indoor air profile view and (b) its equivalent RC-network.

Based on this introductive definition, the Kron's modelling of our room structure will be elaborated in the following section.

III. DEVELOPMENT OF THE ORIGINAL KRON'S MODEL OF THE ROOM THERMAL RESPONSES

The present section develops the description of the classical equivalent thermal network. Through the equivalent graph topology, the thermal Kron's model will be implemented. Then, the TTFs at the different indoor nodes will be established. Before this analytical development, it is worth to introduce in understandable way the methodology of the unfamiliar Kron's method in the following subsection.

A. METHODOLOGY OF THE KRON'S FORMALISM APPLICATION

The unfamiliar Kron's formalism [36] is a particularly efficient approach to model the engineering problem represented as networked systems. However, extra-effort needs to be paid for the non-specialist building design engineer to be familiar to the method. Following this motivation, our research work serves pedagogically to make this power formalism to be open to any engineers.

First and foremost, so far, it is interesting to remind that the Kron's formalism is outstandingly well adapted for electromagnetic circuits. Meanwhile, it contributes indirectly to different applications as social, mechanical, thermal, chemical, etc., uses.

Then, in the practical engineering point of view, the Kron's formalism consists in modelling of any physical problem via the network approach. The analytical theory is the tensorial mathematization of the elementary objects as 1- or 2-rank tensors often named simplex. The system complex can be represented by the simplex interaction with tensorial operations. To summarize the TAN methodology to solve typical thermal problem as the case of our room shown in Figs. 1, we propose the workflow of Fig. 6 [25].

To explain more clearly, the application of Kron's formalism, we can consider the network shown in Fig. 7. The practical methodology to treat this type of graph is explained in the following items:

- The Kron's method should start for the problem formulation which corresponds to the room structure initiated in Figs. 1 for the present study.
- Afterwards, the problem must be geometrized in function of the targeted solution.
- Then, with the basic laws' physics, we can transform the structure into an electrical thermal circuit.
- In the next step of the modeling, the thermal circuit must be translated as a Kron's graph topology. For the better understanding we can look over the two-mesh graph shown in Fig. 6.
- The topological parameter of the graph must be tabulated. For the example, of the case of Fig. 6, the Kron's universe is made of three branches $\{B_1, B_2, B_3\}$. Each branch has an impedance represented by the components denoted (A, B, C). Under the topological parametrization, we can see that this graph is a single network, R, having two nodes, $\{N_1, N_2\}$. In consequence, the number of meshes (M) required to analyze the system is given by this Euler-Poincaré topological invariant formula [31]:

$$M = B - N + R. \tag{6}$$

- From this graph, the systemic analysis can be performed first in the branch space and then, in the mesh space.
- Based on the graph topology, the last phase of the Kron's method can be the mathematization. The most general way of this mathematization should be the tensorial approach in the adequate space (branch, node, summit, mesh ...).

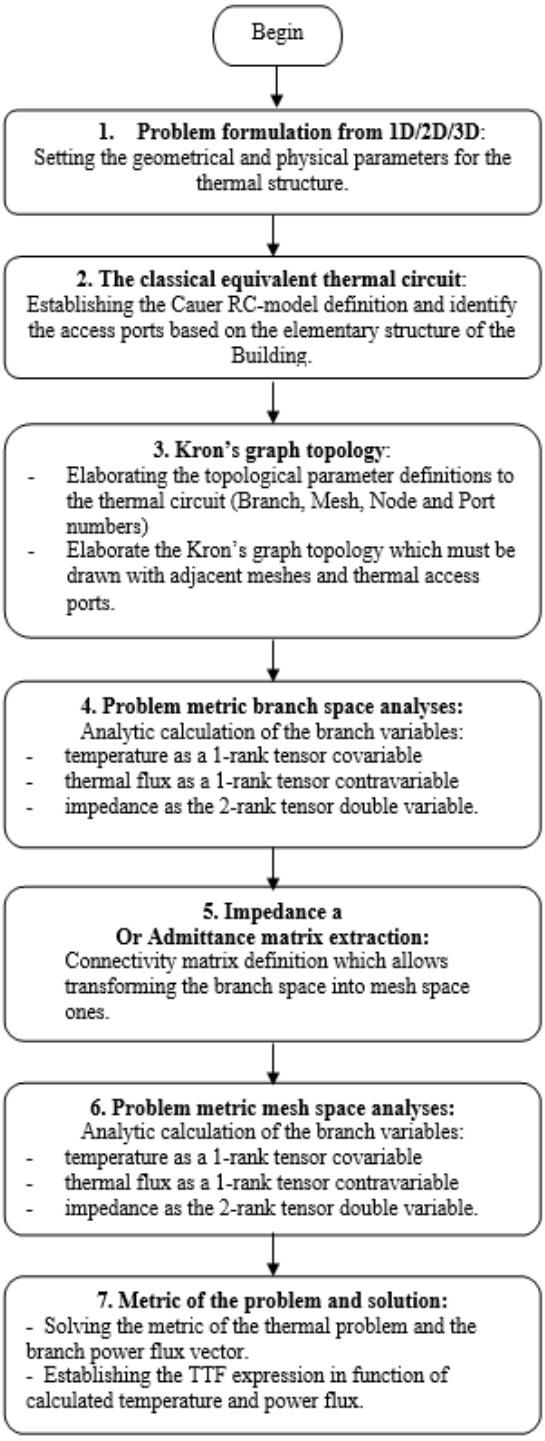

FIGURE 6. Workflow summarizing the main steps of the Kron's method.

B. ELABORATION OF THE THERMAL EQUIVALENT CIRCUIT

The meshing geometrization of the room structure will serve as the initial step of the Kron's modelling. However, for the

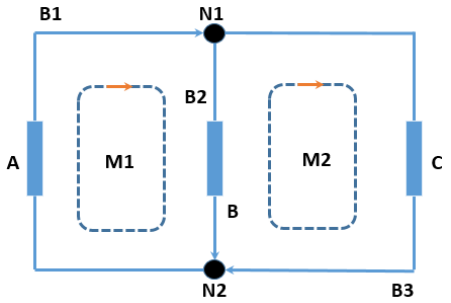

FIGURE 7. Illustration of the Kron's graph with two-mesh structure.

basic understanding, it would be essential to establish the classical thermal circuit based on the RC-network.

1) NODED GEOMETRICAL DESCRIPTION OF THE ROOM STRUCTURE

For a better understanding of the Kron's modelling, we propose to start with the geometrization by considering the meshing related to the door and the wall widths. Accordingly, Fig. 8(a) presents the top view of the room. The external temperature source is naturally induced in the outdoor environment. The t time-dependent instantaneous temperature is represented by $T_{source}(t)$. This source is connected to the three nodes, N_0, which are connected to the outside of the room wall and door. Then, the test points corresponding to the temperatures near the source are denoted by N_1, N_2 and N_3. The medium nodes for the middle plane are indicated by M_1, M_2 and M_3. Then, the far nodes are referenced by F_1, F_2 and F_3.

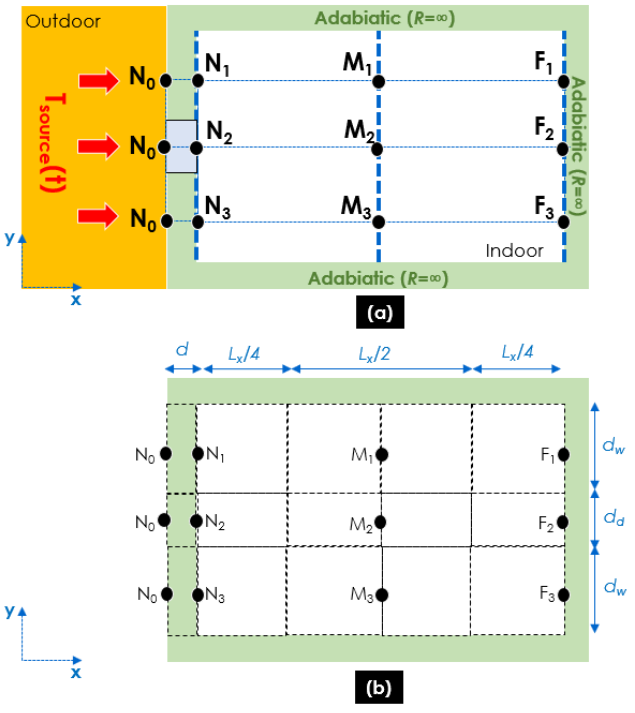

FIGURE 8. Geometrization of the problem: (a) top view and (b) meshed structure of the room.

The structure meshing is configured in Fig. 8(b) by taking into account the wall length, d_w, and door width, d_d. The wall and door thickness are assumed to be equal to d. It can be seen that the axis ($N_2M_2F_2$) constitutes a symmetrical axis of the overall structure. It means that the lateral thermal responses referring to the nodes, N_1 and N_3, M_1 and M_3, and F_1 and F_3, are identical.

From an analytical point of view, the unknown parameters of this thermal modelling problem can be expressed by the components of the following vector:

$$T_{unknowns} = \begin{bmatrix} T(N_1) = T(N_3) \\ T(N_2) \\ T(M_1) = T(M_3) \\ T(M_2) \\ T(F_1) = T(F_3) \\ T(F_2) \end{bmatrix}. \quad (7)$$

Under such formulation, the thermal problem under study can be redrawn as depicted in Fig. 9 by the determination of the multi-port TTF. In brief, the overall room structure under study can be assumed as 7-port system with single input and six outputs.

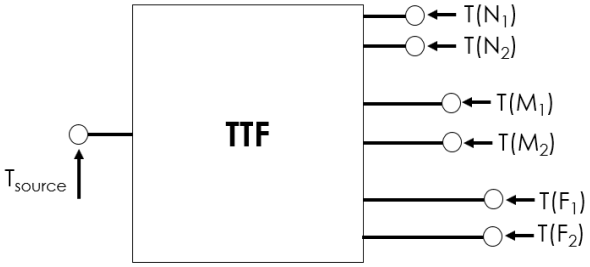

FIGURE 9. Multi-port black box diagram of the room thermal problem.

2) IDENTIFICATION OF NETWORK LUMPED R AND C ELEMENTS

Before the thermal circuit design, the specification of each elementary components between the nodes, N_m, M_m and F_m. ($m = 0, 1, 2, 3$) of the structure shown in Fig. 3 is necessary. Table 1 summarizes these components for three constituting materials, wall, door and indoor air. Each component is

TABLE 1. Parameters of room thermal network.

Material	Connecting nodes	Nature	Parameter
Wall	N_0N_1 and N_0N_3	Resistor	R_w
		Capacitor	C_w
Door	N_0N_2	Resistor	R_d
		Capacitor	C_d
Indoor air	N_mM_m, N_mM_m, (with m=1,2,3) and N_mN_{m+1}, M_mM_{m+1}, F_mF_{m+1} (with m=1,2)	Resistor	R, R_1, R_2, R_3
		Capacitor	C_1, C_2, C_3

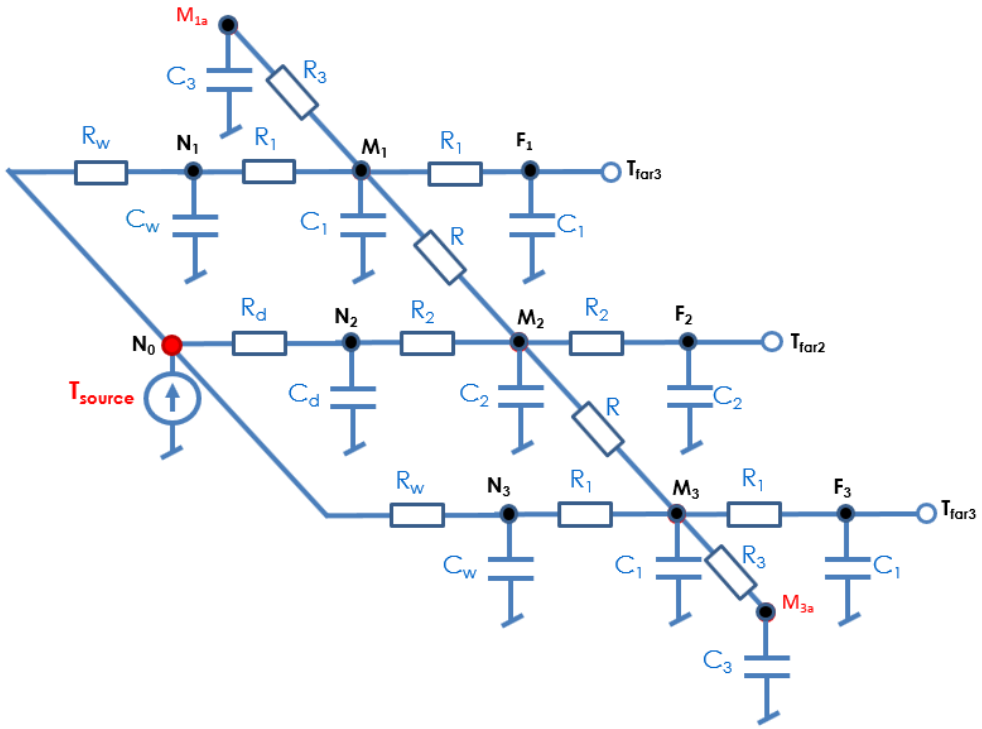

FIGURE 10. Equivalent thermal network of the room meshed structure shown in Fig. 8.

determined by formulas (4) and (5). Let notice that, we have chosen to stay on its components for the sake of simplicity and to avoid unnecessary computational efforts.

3) CIRCUIT DESIGN OF THE ROOM THERMAL NETWORK

The thermal equivalent network is established from the RC-model introduced in Fig. 5(b) applied to the wall, door and meshed indoor air. The circuit design, drawn in Fig. 10, can be understood with the positions of referential nodes, N_m, M_m and F_m ($m = 0, 1, 2, 3$). It is noteworthy that the circuit is built under the reference temperature, T_a, implicitly the potential ground node. The thermal source, T_{source}, is connected to N_0. In the circuit problem, the main unknown parameters are the temperature at the other nodes as indicated in vector (6).

We would like to emphasize herein about the equivalent circuit construction. The design of the circuit approach depicted in Fig. 10 is related to the hypothesis of the temperature source propagation in 1-D in the near zone. The effect of the lateral RC network can be neglected with the considered size of geometrical meshing. In the far zone, we also adopted the adiabatic hypothesis which enables to avoid the temperature change in the far zone corners. In difference to the near and far zone, the middle one is essentially constituted by the air. Therefore, we assumed that in the middle area, the propagation of the temperature from nodes M_1 and M_3 to the lateral walls can be represented by network R_3C_3.

C. IMPLEMENTATION OF THERMAL KRON'S MODELLING

The implementation of the Kron's model is performed via graph topology and the tensorial approach. The next paragraphs develop the detailed expression of the room thermal model.

1) KRON'S GRAPH TOPOLOGY

Fig. 11 represents the Kron's equivalent graph topology of the thermal network introduced in Fig. 10. The circuit design is implemented with the thermal capacitors connected to the ground ambient temperature in virtual 3-D view. This thermal circuit universe is built with the interconnections of branches. In this circuit, each branch is constituted by a thermal resistor or a thermal capacitor. The circuit can also be seen in another space based on the mesh representation. The rigorous Kron's method analysis can be performed with the topological parameters addressed in Table 2.

TABLE 2. Topological parameters.

Designation	Branch	Node	Mesh	Port
Parameter	B	N	M	P
Value	18	8	11	7

Knowing these parameters, the tensorial branch analysis with the Kron's method will be proposed in the next paragraph.

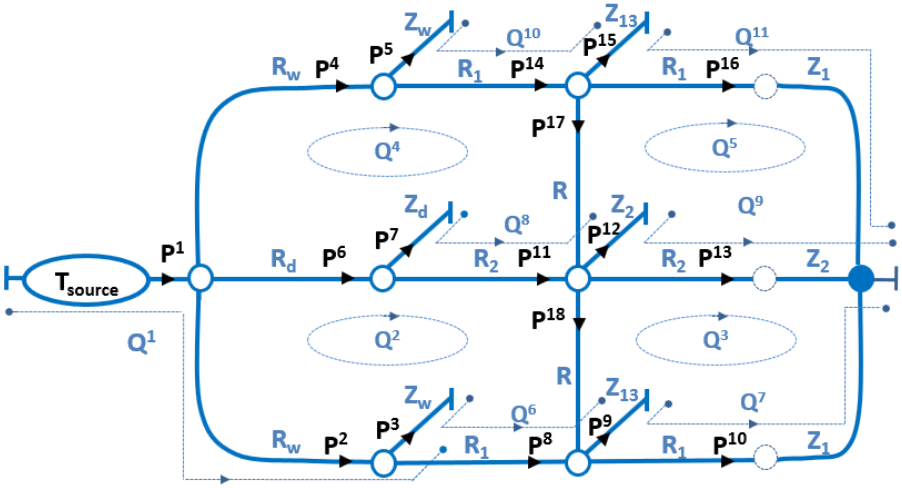

FIGURE 11. Kron's topological graph equivalent to the thermal network introduced in Fig. 8.

2) BRANCH SPACE ANALYSIS

The branch space variable can be referred with the positive integer index, $b = 1, 2, \ldots, B$. As covariable, the branch temperature of the graph introduced in Fig. 11 can be expressed as:

$$T_b = \begin{bmatrix} T_{source} & 0 & \ldots & 0 \end{bmatrix}. \tag{8}$$

The associated dual contravariable is represented by the branch power flux given by:

$$P^b = \begin{bmatrix} P^1 \\ P^2 \\ \vdots \\ P^B \end{bmatrix}. \tag{9}$$

Acting as a lumped circuit, the double covariable thermal branch impedance, is given by the block notation:

$$Z_{bb} = \begin{bmatrix} 0 & 0 & 0 & 0 \\ 0 & [Z_{wall}] & 0 & 0 \\ 0 & 0 & [Z_{door}] & 0 \\ 0 & 0 & 0 & [Z_{air}] \end{bmatrix}. \tag{10}$$

It acts as a diagonal matrix because the circuit does not present any interbranch coupling phenomenon. Each submatrix corresponds to the constituting block of our room structure as the wall, door and indoor air which represented by the branch thermal impedances, respectively:

$$[Z_w] = \begin{bmatrix} R_w & 0 & 0 & 0 \\ 0 & Z_w & 0 & 0 \\ 0 & 0 & R_w & 0 \\ 0 & 0 & 0 & Z_w \end{bmatrix} \tag{11}$$

$$[Z_{door}] = \begin{bmatrix} R_d & 0 \\ 0 & Z_d \end{bmatrix} \tag{12}$$

and the (11×11)-dimension matrix, $[Z_{air}]$ expressed in equation (13), as shown at the bottom of this page. The thermal capacitive impedance elements are defined by:

$$Z_{N_1} = Z_{N_3} = Z_w = \frac{1}{C_w s} \tag{14}$$

$$Z_{N_2} = Z_d = \frac{1}{C_d s} \tag{15}$$

$$Z_{M_1} = Z_{M_3} = Z_{13} \tag{16}$$

$$[Z_{air}] = \begin{bmatrix} R_1 & 0 & 0 & 0 & 0 & 0 & 0 & 0 & 0 & 0 & 0 \\ 0 & Z_{13} & 0 & 0 & 0 & 0 & 0 & 0 & 0 & 0 & 0 \\ 0 & 0 & R_1 + Z_1 & 0 & 0 & 0 & 0 & 0 & 0 & 0 & 0 \\ 0 & 0 & 0 & R_2 & 0 & 0 & 0 & 0 & 0 & 0 & 0 \\ 0 & 0 & 0 & 0 & Z_2 & 0 & 0 & 0 & 0 & 0 & 0 \\ 0 & 0 & 0 & 0 & 0 & R_2 + Z_2 & 0 & 0 & 0 & 0 & 0 \\ 0 & 0 & 0 & 0 & 0 & 0 & R_1 & 0 & 0 & 0 & 0 \\ 0 & 0 & 0 & 0 & 0 & 0 & 0 & Z_{13} & 0 & 0 & 0 \\ 0 & 0 & 0 & 0 & 0 & 0 & 0 & 0 & R_1 + Z_1 & 0 & 0 \\ 0 & 0 & 0 & 0 & 0 & 0 & 0 & 0 & 0 & R & 0 \\ 0 & 0 & 0 & 0 & 0 & 0 & 0 & 0 & 0 & 0 & R \end{bmatrix} \tag{13}$$

$$Z_{M_2} = Z_{F_2} = \frac{1}{C_2 s} \tag{17}$$

$$Z_{M_1} = Z_{F_3} = \frac{1}{C_1 s} \tag{18}$$

$$Z_{13} = \frac{Z_1 Z_3}{Z_1 + Z_3} \tag{19}$$

with

$$Z_1 = \frac{1}{C_1 s} \tag{20}$$

$$Z_3 = R_3 + \frac{1}{C_3 s}. \tag{21}$$

3) MESH SPACE ANALYSIS

The mesh space variable can be referred with the positive integer index, $m = 1, 2, \ldots, M$. Based on the Kron's method, the branch to space conversion of the thermal variables must be performed with the connectivity matrix denoted Ξ_b^m. This matrix enables to realize the following transform of the branch temperature, T_b, and power flux, P^b, into the mesh temperature, W_m, and power flux, Q^m, written as:

$$W_m = \Xi_m^b T_b \tag{22}$$

$$Q^m = \Xi_b^m P^b. \tag{23}$$

The global connectivity matrix of the graph shown in Fig. 8 in function constituting block (door, wall, indoor air) ones is expressed as:

$$\Xi_m^b = \begin{bmatrix} 1 \\ [\Xi_{wall}] \\ [\Xi_{door}] \\ [\Xi_{air}] \end{bmatrix}. \tag{24}$$

The connectivity sub-matrices representing the walls, door and the indoor air are denoted, $[\Xi_{wall}]$, $[\Xi_{door}]$ and $[\Xi_{air}]$, respectively. The expressions of these sub-matrices are given in equations (25), (26) and (27), as shown at the bottom of this page, respectively. In this notation, the ternary elements, "−1", "0" and "1" corresponds to the coefficients of the branch flux in function of mesh fluxes with respect the second Kirchoff circuit node's law.

It can be demonstrated that the mesh temperature covariable is expressed as:

$$W_m = \begin{bmatrix} T_{source} & 0 & \ldots & 0 \end{bmatrix}. \tag{28}$$

We point out that according to the tensor algebra, Ξ_m^b represents the matrix transpose of Ξ_b^m. Substantially, the mesh impedance of our thermal graph can be obtained from the relationship:

$$\Omega_{mn} = \Xi_m^b Z_{bb} \Xi_n^b. \tag{29}$$

It is noteworthy that the subscript, n, plays the same role as m. Therefore, it can be defined as a positive integer index, $n = 1, 2, \ldots, M$.

4) EXPRESSIONS OF TTF VECTORS

Based on the previously expressed mesh impedance, the metric of the thermal problem can be formulated by:

$$W_m = \Omega_{mn} Q^n. \tag{30}$$

Substituting the mesh power flux given in (23) into the previous metric, it yields the following tensorial solution of the posed problem:

$$W_m = \Omega_{mn} \Xi_b^n P^b \tag{31}$$

Therefore, the branch power flux vector is:

$$P^b = \Xi_n^b Y^{nm} W_m \tag{32}$$

where we expressed the mesh admittance as:

$$Y^{nm} = \Omega_{mn}^{-1}. \tag{33}$$

$$[\Xi_{wall}] = \begin{bmatrix} 1 & -1 & 0 & 0 & 0 & 0 & 0 & 0 & 0 & 0 & 0 \\ 1 & 0 & 0 & 0 & 0 & -1 & 0 & 0 & 0 & 0 & 0 \\ 0 & 0 & 0 & 1 & 0 & 0 & 0 & 0 & 0 & 0 & 0 \\ 0 & 0 & 0 & 0 & 0 & 0 & 0 & 0 & 0 & -1 & 0 \end{bmatrix} \tag{25}$$

$$[\Xi_{door}] = \begin{bmatrix} 0 & 1 & 0 & -1 & 0 & 0 & 0 & 0 & 0 & 0 & 0 \\ 0 & 0 & 0 & 0 & 0 & 0 & 0 & -1 & 0 & 0 & 0 \end{bmatrix} \tag{26}$$

$$[\Xi_{air}] = \begin{bmatrix} 0 & -1 & 0 & 0 & 0 & 1 & 0 & 0 & 0 & 0 & 0 \\ 0 & 0 & 0 & 0 & 0 & 1 & -1 & 0 & 0 & 0 & 0 \\ 0 & 0 & -1 & 0 & 0 & 0 & 1 & 0 & 0 & 0 & 0 \\ 0 & 1 & 0 & -1 & 0 & 0 & 0 & 1 & 0 & 0 & 0 \\ 0 & 0 & 0 & 0 & 0 & 0 & 0 & 1 & -1 & 0 & 0 \\ 0 & 0 & 1 & 0 & -1 & 0 & 0 & 0 & 1 & 0 & 0 \\ 0 & 0 & 0 & 1 & 0 & 0 & 0 & 0 & 0 & 1 & 0 \\ 0 & 0 & 0 & 0 & 0 & 0 & 0 & 0 & 0 & 1 & -1 \\ 0 & 0 & 0 & 0 & 1 & 0 & 0 & 0 & 0 & 0 & 1 \\ 0 & 0 & 0 & 1 & -1 & 0 & 0 & 0 & 0 & 0 & 0 \\ 0 & 1 & -1 & 0 & 0 & 0 & 0 & 0 & 0 & 0 & 0 \end{bmatrix} \tag{27}$$

It means that the TTFs associated to the temperature vector given in equation (7) can be determined by:

$$\begin{cases} TTF_{N_1}(s) = TTF_{N_3}(s) = \dfrac{Z_w(s)P^5(s)}{T_{source}(s)} \\ TTF_{N_2}(s) = \dfrac{Z_d(s)P^7(s)}{T_{source}(s)} \\ TTF_{M_1}(s) = TTF_{M_3}(s) = \dfrac{Z_{13}(s)P^{15}(s)}{T_{source}(s)} \\ TTF_{M_2}(s) = \dfrac{Z_2(s)P^{12}(s)}{T_{source}(s)} \\ TTF_{F_1}(s) = TTF_{F_3}(s) = \dfrac{Z_1(s)P^{16}(s)}{T_{source}(s)} \\ TTF_{F_2}(s) = \dfrac{Z_2(s)P^{13}(s)}{T_{source}(s)}. \end{cases} \tag{34}$$

To verify the effectiveness of the developed thermal Kron's method, these tensorial analytical expressions were programmed in Matlab environment. The investigated results will be described in the next section.

IV. VALIDATION OF RESULTS

To verify the feasibility of the thermal Kron's model, the present section introduces the room structure proof of concept (POC). The validations are based on frequency and time domain analyses. Comparisons between calculated results and simulations are explored in this section. The model was implemented as a Matlab routine program. The simulations are carried out in the environment of electronic circuit simulator commercial tool ADS® from Keysight Technologies®. Then, the discussed results will be examined in the next subsections.

A. POC DESCRIPTION

Before the exploration of the simulated results, it is worth to describe the thermal structure POC. As aforementioned, the present study is assumed under the hypothesis cited in Section II.A and the door is in a closed state.

1) DESCRIPTION OF THE POC PHYSICAL PARAMETERS

The overall geometrical sizes of the thermal structure were introduced earlier in Fig. 1. In the present case of study, we assume that the wall and wood are made in unfired clay bricks [34] and wood across the grain [35]. Table 3 indicates the physical parameters of each material constituting these elements.

Based on these specifications, the R and C thermal lumped components constituting the branch of the POC circuit were determined by means of equations (4) and (5), respectively.

We underline that the thermal resistor and thermal capacitors depend on the terminal nodes of meshing element. Subsequently, the thermal resistors were calculated as follows:

$$R_w = \frac{d}{\lambda_w d_w L_x} \tag{35}$$

$$R_d = \frac{d}{\lambda_d d_d L_x} \tag{36}$$

TABLE 3. Physical parameters of the thermal circuit POC representing the room structure.

Structure	*Designation*	*Parameters*	*Values*
Wall	Geometrical sizes with propagation $N_0 \rightarrow N_1$	$s_1=d_w$	2 m
		$s_2=L_z$	2.3 m
		$s_3=d$	0.104 m
	Thermal conductivity	λ_w	0.9 W/m/K
	Specific heat	h_w	545 J/kg/K
	Mass density	ρ_w	1788 kg/m^3
Door	Geometrical sizes with propagation $N_0 \rightarrow N_2$	$s_1=d_d$	1 m
		$s_2=L_z$	2.3 m
		$s_3=d$	0.05 m
	Thermal conductivity	λ_d	0.2 W/m/K
	Specific heat	h_d	1400 J/kg/K
	Mass density	ρ_d	800 kg/m^3
Air	Thermal conductivity	λ_a	0.026 W/m/K
	Specific heat	h_a	1007 J/kg/K
	Mass density	ρ_a	1.16 kg/m^3
	Geometrical sizes with propagation $N_1 \rightarrow M_1$	$s_1=d_w$	2 m
		$s_2=L_z$	2.3 m
		$s_3=L_x/2$	2 m
	Geometrical sizes with propagation $N_2 \rightarrow M_2$	$s_1=d_d$	1 m
		$s_2=L_z$	2.3 m
		$s_3=L_x/2$	2 m
	Geometrical sizes with propagation $N_3 \rightarrow M_3$	$s_1=d_w$	2 m
		$s_2=L_z$	2.3 m
		$s_3=L_x/2$	2 m
	Geometrical sizes with propagation $M_1 \rightarrow F_1$	$s_1=d_w$	2 m
		$s_2=L_z$	2.3 m
		$s_3=L_x/2$	2 m
	Geometrical sizes with propagation $M_2 \rightarrow F_2$	$s_1=d_d$	1 m
		$s_2=L_z$	2.3 m
		$s_3=L_x/2$	2 m
	Geometrical sizes with propagation $M_3 \rightarrow F_3$	$s_1=d_w$	2 m
		$s_2=L_z$	2.3 m
		$s_3=L_x/2$	2 m
	Geometrical sizes with propagation, $M_2 \rightarrow M_1$, and $M_2 \rightarrow M_3$	$s_1=L_x/4$	2 m
		$s_2=L_z$	2.3 m
		$s_3=(d_w+d_d)/2$	1.5 m
	Geometrical sizes with propagation, $M_1 \rightarrow M_{1a}$, and $M_3 \rightarrow M_{3a}$	$s_1=L_x/2$	2 m
		$s_2=L_z$	2.3 m
		$s_3=d_w/2$	1 m

$$\begin{cases} R = \dfrac{2(d_w + d_d)}{\lambda_a L_x L_z} \\ R_1 = \dfrac{L_x}{2\lambda_a d_w L_z} \\ R_2 = \dfrac{L_x}{2\lambda_a d_d L_z} \\ R_3 = \dfrac{d_w}{\lambda_a L_x L_z}. \end{cases} \tag{37}$$

The associated thermal capacitors are given by:

$$C_w = \rho_w h_w d_w L_z d \tag{38}$$

$$C_d = \rho_d h_d d_d L_z d \tag{39}$$

$$\begin{cases} C_1 = \dfrac{1}{2}\rho_a h_a d_w L_z L \\ C_2 = \dfrac{1}{2}\rho_a h_a d_d L_z L_x \\ C_3 = \dfrac{1}{4}\rho_a h_a L_x L_z d_w. \end{cases} \tag{40}$$

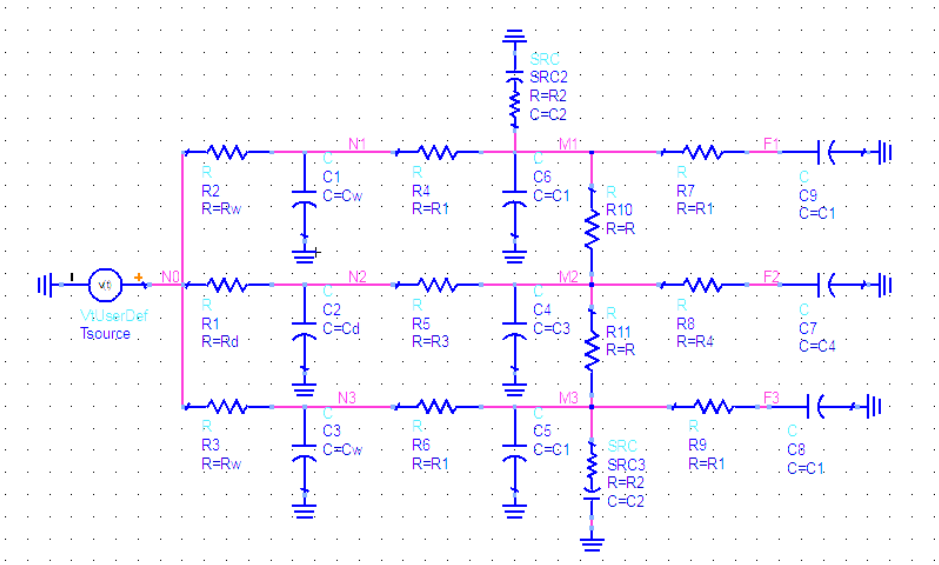

FIGURE 12. Design of simulated thermal circuit POC.

TABLE 4. RC parameters of the constituting nodded elements.

Structure	*Designation*	*Parameters*	*Values*
Wall	Thermal resistor	R_w	0.025 K/W
	Thermal capacitor	C_w	466.18 kJ/K
Door	Thermal resistor	R_d	0.109 K/W
	Thermal capacitor	C_d	129 kJ/K
Air	Thermal resistor $N_1 \rightarrow M_1$ and $M_1 \rightarrow F_1$	R_1	17 K/W
	Thermal capacitor $N_1 \rightarrow M_1$ and $M_1 \rightarrow F_1$	C_1	10.7 kJ/K
	Thermal resistor $N_2 \rightarrow M_2$ and $M_2 \rightarrow F_2$	R_2	33 K/W
	Thermal capacitor $N_2 \rightarrow M_2$ and $M_2 \rightarrow F_2$	C_2	5.373 kJ/K
	Thermal resistor $M_1 \rightarrow M_2$	R	12.5 K/W
	Thermal resistor $M_1 \rightarrow M_{1a}$, and $M_3 \rightarrow M_{3a}$	R_3	8.36 K/W
	Thermal capacitor$M_1 \rightarrow M_{1a}$, and $M_3 \rightarrow M_{3a}$	C_3	5.373 KJ/K

2) DESCRIPTION OF THE SIMULATED THERMAL CIRCUIT DESIGN

The POC schematic of the thermal circuit design is displayed in Fig. 12. This circuit was drawn in the SPICE environment, usually exploited to the electrical and electronic circuit designs. The temperature excitation source is represented by the voltage source connected to the node, N_0. The unknown indoor temperatures correspond to the voltages at the other nodes indicated by $Near_{1,2}$, $Mid_{1,2}$ and $Far_{1,2}$ of the POC circuit. During the simulations, the voltages at these nodes can be assessed and compared with the excitation one in order to determine the TTFs.

The comparisons between calculated and simulated frequency domain results will be examined in the next subsection.

B. FREQUENCY DOMAIN RESULTS

The present case of the frequency domain is rarely elaborated in the area of thermal building engineering. One of the original points of Kron's method is the possibility to perform such a study and understanding the behavior of the thermal structure constituting the room. The following results of the frequency domain are based on Matlab computation of the Kron's model compared to simulations with the SPICE AC analyses.

1) TTF MAGNITUDES

To visualize the significant behaviors of the TTFs, two range of frequencies were considered. In the first case, the frequency domain was investigated in the frequency band up to $f_{max} = 10\ \mu$Hz. In the other case, the analysis is performed up to $f_{max} = 100\ \mu$Hz. Linear and semi-logarithmic plots of magnitudes were presented for a better understanding of the thermal responses at the different test points.

Figs. 13 and Figs. 14 present the comparisons between the calculated and simulated TTFs at the near, mid and far positions. The simulations are plotted in solid lines and the Kron's method calculated ones are shown in dotted lines. As expected, the Kron's model is in very good agreement with the SPICE simulation. It is noteworthy that as seen in Fig. 13(a) and in Fig. 14(a), in the near side of the wall and door, the TTF is close to the unity. More generally, at extremely low frequencies below 100 nHz, all the TTFs can be assumed as equal to unity. However, in the mid and far TTF responses plotted in Figs. 13(b) and 14(b), and in Figs. 13(c) and 14(c), respectively, we have a typical

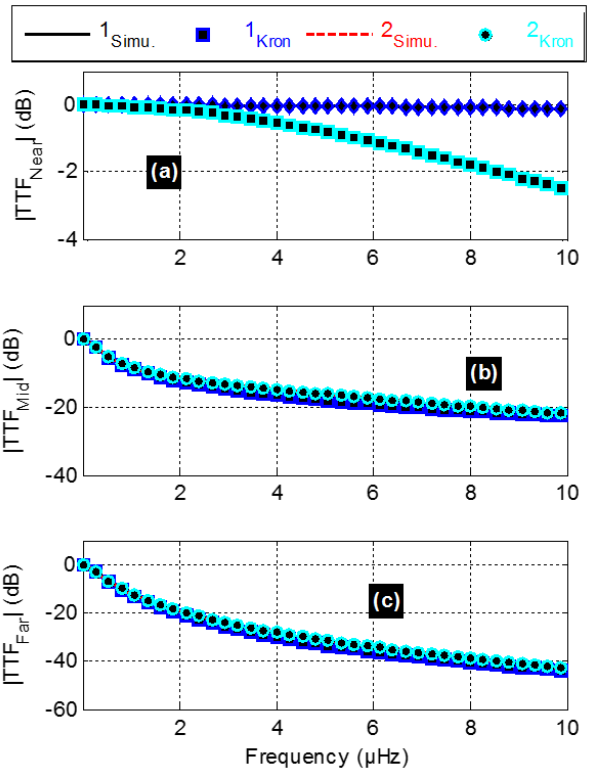

FIGURE 13. Linear plot of simulated and calculated TTF magnitudes in (a) near, (b) middle and (c) far test nodes up to $f_{max} = 10$ μHz.

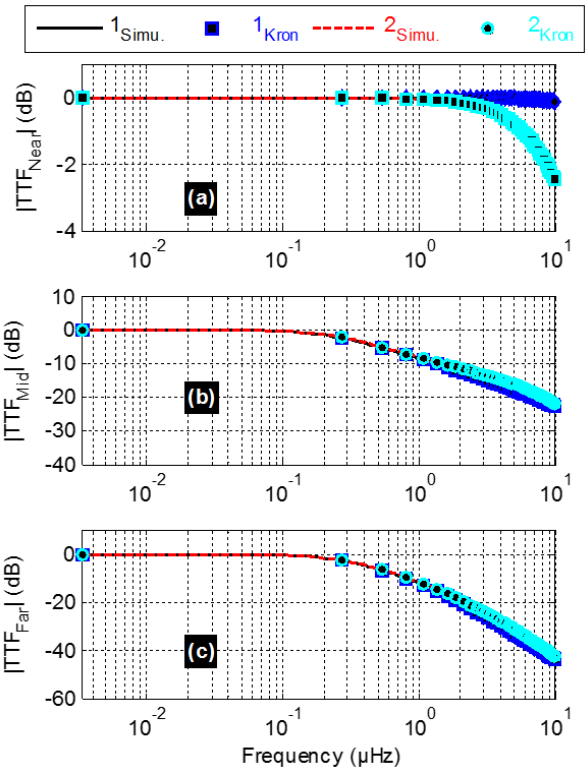

FIGURE 14. Semi-logarithmic plot of simulated and calculated TTF magnitudes in (a), near, (b) middle and (c) far test nodes up to $f_{max} = 10$ μHz.

low-frequency thermal behavior. The mid TTF attenuates more than 20 dB at higher frequencies more than 5 μHz as depicted in Fig. 14(b). However, the far TTF attenuates more than 20 dB only 2 μHz. Then, at extremely high frequencies, the attenuation increases with slope 20 dB/decade.

The magnitude responses in linear and semi-logarithmic plots respecting the wider frequency analyses up to $f_{max} = 100$ μHz are exposed in Figs. 15 and in Figs. 16, respectively. It can be understood from Fig. 15(a) that the temperature thorough the door is much higher than the temperature through the lateral walls. Along the symmetrical axis, the attenuation remains lower than 10 dB up to 100 μHz. However, the wall TTF has reached 20 dB attenuation only at about 60 μHz. Then, as seen in Figs. 15(b) and in Figs. 16(b), the mid TTF attenuation reaches 40 dB at 30 μHz. Then, strong attenuation of about 50 dB is realized with the far TTF beyond 20 μHz.

2) TTF PHASE RESPONSES

These AC analyses guarantee that the fast variation of the temperature cannot propagate through the considered wall and door structures. In the worst case of thermal shielding, the propagation can be limited in the near zone of the source.

The phase responses of the TTFs were explored only in linear plots because the phase information at lower frequencies is almost trivial and near zero. However, the two cases of the frequency limits, $f_{max} = 10$ μHz to $f_{max} = 100$ μHz were also considered for the present AC analyses.

Figs. 17 and Figs. 18 present the comparisons between the calculated and simulated TTF phases. Once again, it can be underlined that the Kron's calculated results are in very good correlation with the simulations. For all cases of TTFs, the phases are decreasing with the frequency. This behavior corresponds to the phase responses of typical linear passive systems as low-pass filters. The phase shifts of the near zone in the lateral indoor part are limited to 20° below 10 μHz. However, the symmetrical axis is almost two times higher. As depicted in Fig. 17(b) and in Fig. 17(c), the mid and far TTF phase shifts exceed 100° beyond 7 μHz and 1 μHz, respectively.

The increase of the TTF phase shifts for all positions is confirmed by Figs. 18. For further validation of the previous simulations, transient analyses were also carried out. The next subsections describe the obtained results.

C. TIME DOMAIN RESULTS

The present thermal time domain analyses are performed based on the consideration of unit step and arbitrary waveform excitation temperatures. The reference ambient temperature was fixed to $T_a = 20$°C for the time domain investigation. Only simulation results are exposed in this case of analysis. For the better understanding about the transient behavior of indoor temperature in the different zones

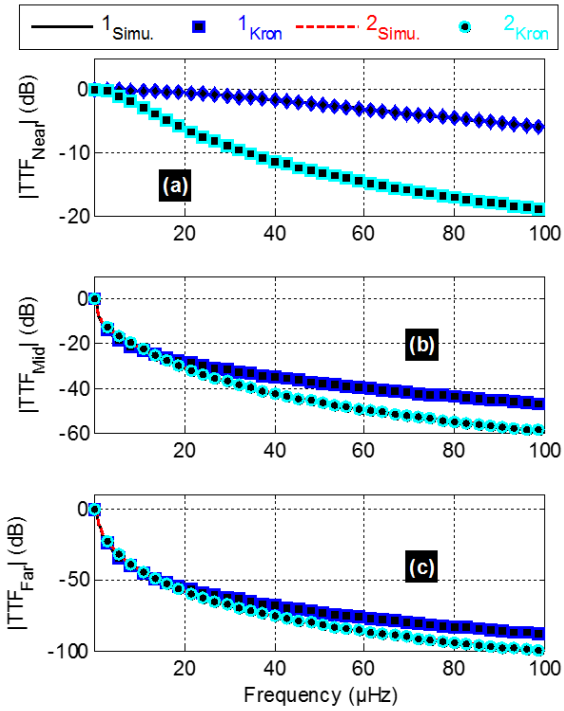

FIGURE 15. Linear plot of simulated and calculated TTF magnitudes in (a), near, (b) middle and (c) far test nodes up to $f_{max} = 100$ μHz.

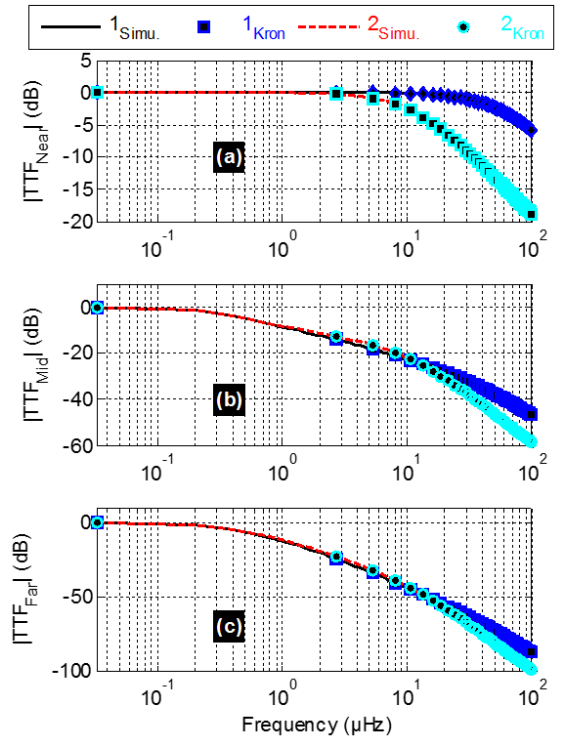

FIGURE 16. Semi-logarithmic plot of simulated and calculated TTF magnitudes in (a), near, (b) middle and (c) far test nodes up to $f_{max} = 100$ μHz.

(near, mid and far), the present time-domain analyses were performed under two different time windows with $t_{max} = 5$ hours and also, $t_{max} = 500$ hours.

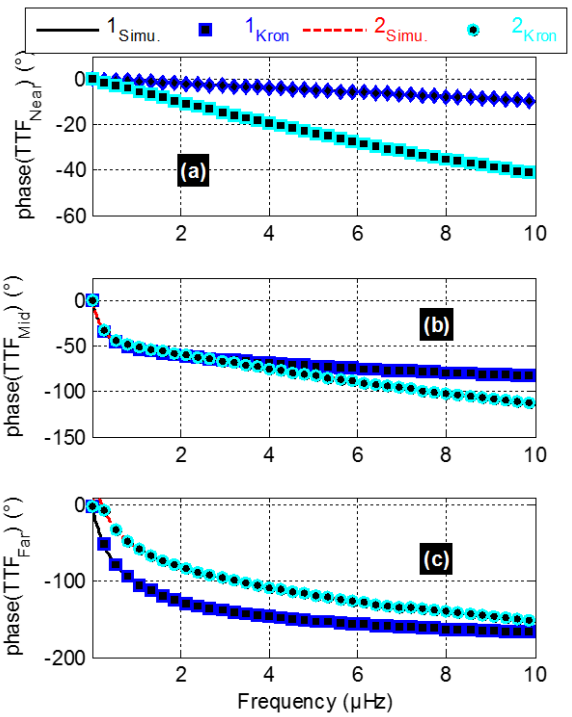

FIGURE 17. Comparisons of simulated and calculated TTF phases in (a), near, (b) middle and (c) far test nodes up to $f_{max} = 10$ μHz.

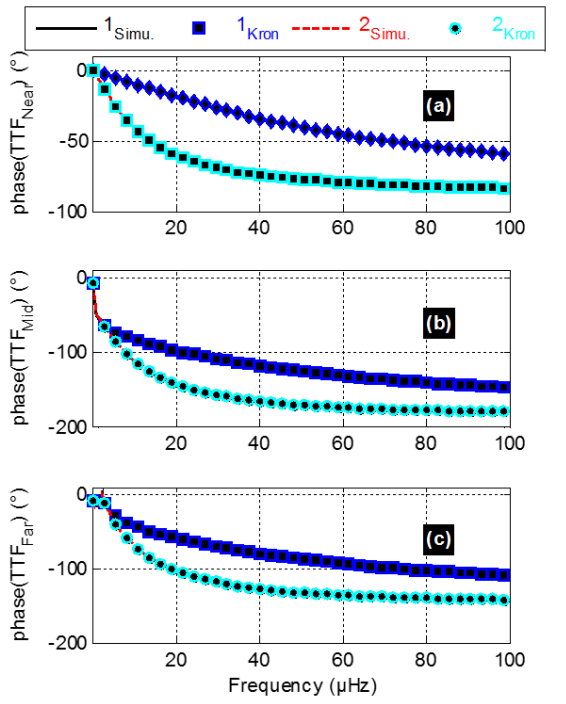

FIGURE 18. Comparisons of simulated and calculated TTF phases in (a), near, (b) middle and (c) far test nodes up to $f_{max} = 100$ μHz.

1) UNIT-STEP EXCITATION TIME-DOMAIN RESULTS

In this case, the excitation signal corresponds to a unit-step temperature with $T_{min} = T_a$ and $T_{max} = 40$°C.

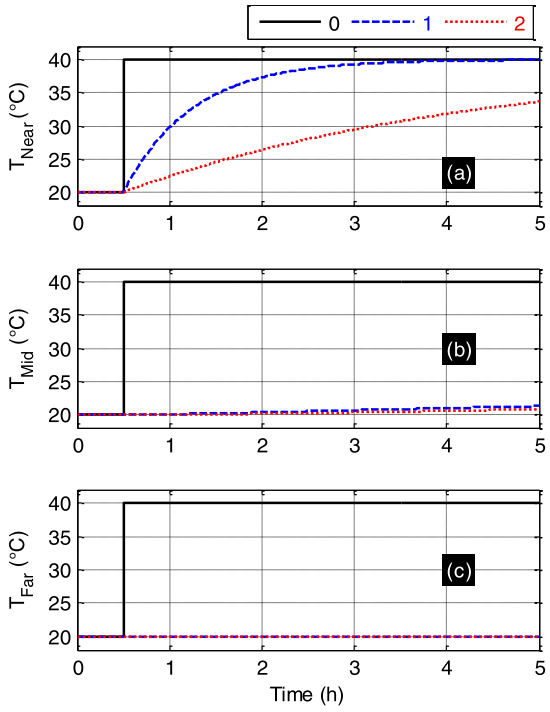

FIGURE 19. Unit-step responses of simulated and calculated thermal network: (a), near, (b) middle and (c) far test node solver short time window.

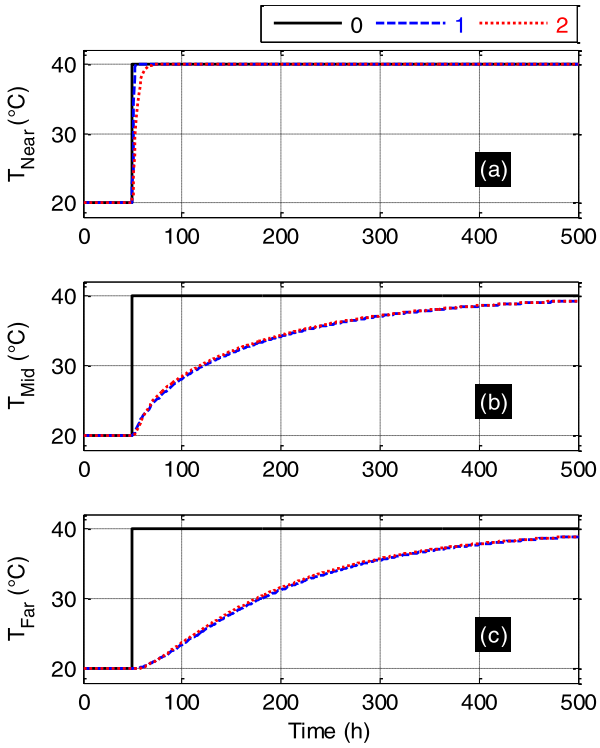

FIGURE 20. Unit-step responses of simulated and calculated thermal network: (a), near, (b) middle and (c) far test nodes over long-time window.

Figs. 19 present the transient analysis with $t_{max} = 5$ hours. The sampling time was fixed equal to 30 seconds. As depicted in Fig. 19(a), the symmetrical axis and lateral near zone temperature reaches the half amplitude equal to 30°C, at about 0.5 hours and 2.5 hours, respectively. However, as illustrated in Fig. 19(b) and in Fig. 19(c), the responses at the mid and far zones are negligible, the temperatures are almost kept to T_a. It points out that the airflow pattern during was neglected in the present case of study.

To visualize the mid and far zone responses, the unit step transient results up to $t_{max} = 500$ hours are introduced in Figs. 20. It can be emphasized that the mid zone temperature reaches the half amplitude only after 70 hours as seen in Fig. 20(b). Fig. 20(c) highlights that the half amplitude can be reached only after 120 hours. This long-time range time domain analyses explain that the temperature in the far zone of the source are almost same for F_1 and F_2.

2) ARBIRARY WAVEFORM EXCITATION TIME-DOMAIN RESULTS

The present time domain analysis is carried out by considering an arbitrary waveform temperature. The same as the previous unit step analyses, the two different time ranges were considered. This time sampling was chosen similarly to the unit step response analysis.

Figs. 21 show the simulated transient results for $t_{max} = 5$ hours. We emphasize that in the considered time range, as shown in Fig. 21(a), the temperature variation is considerably smoothed in the near zone. The indoor

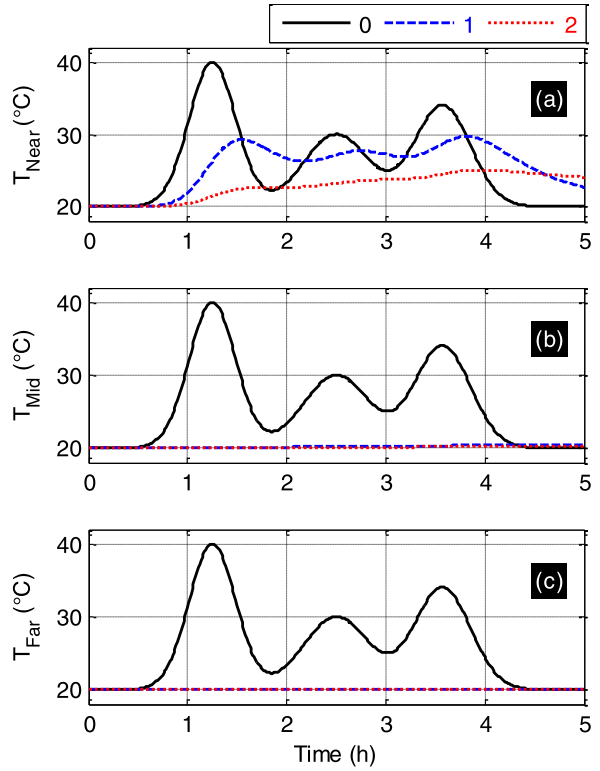

FIGURE 21. Arbitrary waveform temperature responses of simulated and calculated thermal network: (a), near, (b) middle and (c) far test nodes over short time window.

temperature does not exceed the amplitude 40°C. However, as illustrated in Fig. 21(b) and in Fig. 21(c), the mid and far

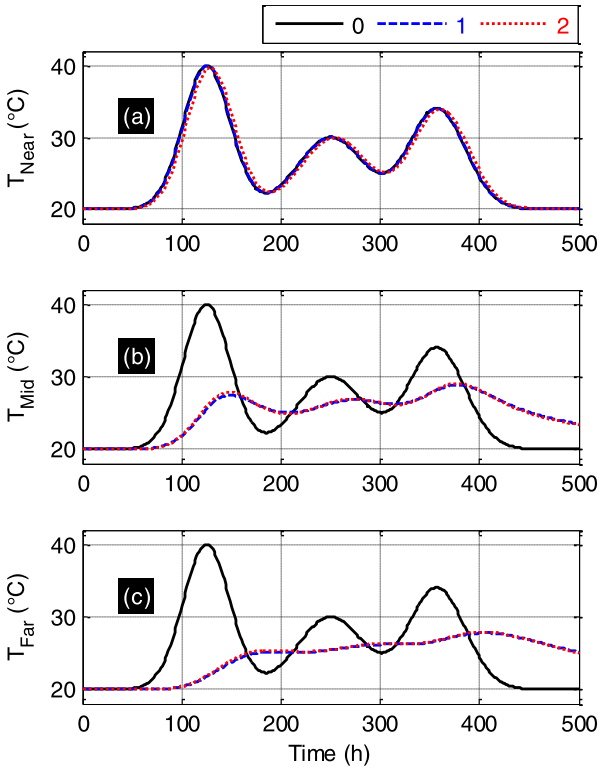

FIGURE 22. Arbitrary waveform temperature responses of simulated and calculated thermal network: (a), near, (b) middle and (c) far test nodes over long-time window.

zone temperatures are remained unchanged as predicted in the unit step time response of the previous paragraph.

The transient responses with $t_{max} = 500$ hours are displayed in Figs. 22. The near zone responses of Figs. 22(a) highlights that the transfer function is close to unity because the signals are extremely slow. However, the mid and far zone transient responses of Fig. 22(b) and Fig. 22(c) highlight that the temperature responses are smoothed. Only half of the maximal amplitudes are reached. With the explored test case of Figs. 2, the minimal, maximal and mean resultant of the temperatures at each node is recapitulated in Table 5.

TABLE 5. Minimal, maximal and mean values of each node temperature (in °C) corresponding to $t_{max} = 500$ hours.

Node	Min.	Max.	Mean
N_1	20	39.9	25.9
N_2	20	39.7	25.9
Difference	0	0.2	0
M_1	20	28.8	24.9
M_2	20	29	24.9
Difference	0	-0.2	0
F_1	20	27.8	24.4
F_2	20	27.9	24.4
Difference	0	-0.1	0

D. ADVANTAGES AND DRAWBACKS OF THE THERMAL KRON'S MODEL

The same as all modelling methods, the developed Kron's thermal method presents certain advantages and drawbacks.

The main benefits of the Kron's tensorial approach compared to the thermal building 3-D computational methods are:

- Inexistence of pre-processing time to design,
- Easiness of implementation as a graph topology,
- Possibility to consider different parameters which can be assumed as tensorial variables,
- Feasibility of analyses in both frequency and time domains,
- And very fast computation time.

However, the weaknesses of the Kron's method are:

- Necessitate a good back ground in TAN approach which is not always familiar to the building engineers,
- And the dependence to the approximation of R and C elements.

Behind the present feasibility study, further investigation must be conducted in the future for more complex building in different seasons of various rural and urban applications.

V. CONCLUSION

An original modelling method of temperature propagation through building room is investigated. The model is based on the Kron's method applied to RC thermal network. After the classical thermal circuit introduction, the Kron's graph is elaborated. Then, the thermal circuit was analyzed in the branch and mesh spaces. Then, the thermal metric of the circuit is compactly expressed in tensorial notation. The main solution of the thermal problem is formulated with the TTF at different indoor test points identified as temperature nodes.

The feasibility of the thermal Kron's modelling was verified by SPICE simulation of a single door room. As expected, a good correlation between the frequency responses of the TTF at near, middle and far positions of the door was obtained.

From practical point of view, the developed Kron's model is dedicated to the building design engineers who need to evaluate quickly the thermal performances of a room or more complex building. It presents the following benefits. The model enables:

- To compare the effect of the materials and the building geometry.
- To manage the building thermal flows in a general manner.
- The perform the feasibility study which is useful to design and control heating and cooling systems in the built environment.

Similar to all pioneer research work on preliminary understandability and feasibility, the present study on unfamiliar modelling method is validated with intentionally simple proof-of-concept. Meanwhile, in the near future, a significant research work should be made for the application exploitation to real cases of building. Under this perspective, further work will be made to develop an operational tool based on the Kron's model.

REFERENCES

[1] (2007). *Housing, Energy and Thermal Comfort: A Review of 10 Countries Within the WHO European Region, WHO/Europe—World, EUR/06/5072464*. Accessed: Jul. 2020. [Online]. Available: http://www.euro.who.int/pubrequest
[2] H. Ritchie and M. Roser. (Sep. 2018). *Urbanization*. Accessed: Jul. 2020. [Online]. Available: https://ourworldindata.org/urbanization
[3] Vivint Smart Home. (May 2019). *What's the Ideal Room Temperature for Comfortable Living?* Accessed: Jul. 2020. [Online]. Available: https://www.vivint.com/resources/article/best-home-room-temperature
[4] M. A. Humphreys, "The dependence of comfortable temperatures upon indoor and outdoor climates," in *Studies in Environmental Science*, vol. 10, Wrocław, Poland: Wroclaw Technical Univ. Press, 1981, ch. 15, pp. 229–250.
[5] D.-M. Han and J.-H. Lim, "Smart home energy management system using IEEE 802.15.4 and zigbee," *IEEE Trans. Consum. Electron.*, vol. 56, no. 3, pp. 1403–1410, Aug. 2010.
[6] M. Ozel and K. Pihtili, "Optimum location and distribution of insulation layers on building walls with various orientations," *Building Environ.*, vol. 42, no. 8, pp. 3051–3059, Aug. 2007.
[7] A. H. Hafez, "Integrating building functions into massive external walls," in *Architecture and the Building Environment*. Rotterdam, The Netherlands: Sirene Ontwerpers, May 2016.
[8] S. Zahiri and H. Altan, "Improving energy efficiency of school buildings during winter season using passive design strategies," *Sustain. Buildings*, vol. 5, no. 1, pp. 1–14, Mar. 2020.
[9] G. Augenbroe, "Trends in building simulation," *Energy Environ.*, vol. 37, nos. 8–9, pp. 891–901, Aug./Sep. 2002.
[10] G. Lefebvre, J. Bransier, and A. Neveu, "Simulation of the thermal behaviour of a room by reduced order numerical methods," *Revue Generale de Thermique*, vol. 34, no. 26, pp. 106–114, 1987.
[11] J. Clarke, *Energy Simulation in Building Design*. Oxford, U.K.: Butterworth-Heinemann, 2001.
[12] V. Garg, K. Chandrasen, J. Mathur, S. Tetali, and A. Jawa, "Development and performance evaluation of a methodology, based on distributed computing, for speeding EnergyPlus simulation," *J. Building Perform. Simul.*, vol. 4, no. 3, pp. 257–270, Sep. 2011.
[13] M. T. Radosevic, J. L. M. Hensen, and A. J. T. M. Wijsman, "Distributed building performance simulation—A novel approach to overcome legacy code limitations," *HVACR Res.*, vol. 12, pp. 621–640, Jul. 2006.
[14] M. H. Benzaama, L. H. Rajaoarisoa, B. Ajib, and S. Lecoeuche, "A data driven methodology to predict thermal behavior of residential buildings using piecewise linear models," *J. Building Eng.*, Aug. 2020, Art. no. 101523.
[15] F. Sehar, M. Pipattanasomporn, and S. Rahman, "A peak-load reduction computing tool sensitive to commercial building environmental preferences," *Appl. Energy*, vol. 161, pp. 279–289, Jan. 2016.
[16] K. K. Andersen, H. Madsen, and L. Hansen, "Modelling the heat dynamic of a building using stochastic differential equations," *Energy Buildings*, vol. 31, pp. 13–24, Jan. 2000.
[17] F. Déqué, F. Ollivier, and A. Poblador, "Grey boxes used to represent buildings with a minimum number of geometric and thermal parameters," *Energy Buildings*, vol. 31, no. 1, pp. 29–35, Jan. 2000.
[18] K. Deng, P. Barooah, P. G. Mehta, and S. P. Meyn, "Building thermal model reduction via aggregation of states," in *Proc. Amer. Control Conf. (ACC)*, Baltimore, MD, USA, Jun./Jul. 2010, pp. 5118–5123.
[19] J. R. Dobbs and B. M. Hencey, "Automatic model reduction in architecture: A window into building thermal structure," in *Proc. 5th Nat. Conf. IBPSA-USA*, Madison, WI, USA, Aug. 2012, pp. 562–568.
[20] G. Fraisse, C. Viardot, O. Lafabrie, and G. Achard, "Development of a simplified and accurate building model based on electrical analogy," *Energy Buildings*, vol. 34, no. 10, pp. 1017–1031, Nov. 2002.
[21] K. J. Kircher and K. M. Zhang, "On the lumped capacitance approximation accuracy in RC network building models," *Energy Buildings*, vol. 108, pp. 454–462, Dec. 2015.
[22] A.-H. Deconinck and S. Roels, "Comparison of characterisation methods determining the thermal resistance of building components from onsite measurements," *Energy Buildings*, vol. 130, pp. 309–320, Oct. 2016.
[23] M. Lauster, J. Teichmann, M. Fuchs, R. Streblow, and D. Mueller, "Low order thermal network models for dynamic simulations of buildings on city district scale," *Building Environ.*, vol. 73, pp. 223–231, Mar. 2014.
[24] A. Bagheri, V. Feldheim, and C. S. Loakimidis, "On the evolution and application of the thermal network method for energy assessments in buildings," *Energies*, vol. 11, no. 4, pp. 1–20, Apr. 2018.
[25] B. Ravelo, L. Rajaoarisoa, and O. Maurice, "Thermal modelling of multilayer walls for building retrofitting," *J. Building Eng.*, vol. 29, May 2020, Art. no. 101126.
[26] J. Berger, S. Gasparin, D. Dutykh, and N. Mendes, "On the comparison of three numerical methods applied to building simulation: Finite-differences, RC circuit approximation and a spectral method," *Building Simul.*, vol. 13, no. 1, pp. 1–18, Feb. 2020.
[27] G. Kron, *Tensor Analysis of Networks*. New York, NY, USA: Wiley, 1939.
[28] O. Maurice, *Elements of Theory for Electromagnetic Compatibility and Systems*. Aix en Provence, France: Bookelis, 2017.
[29] O. Maurice, A. Reineix, P. Durand, and F. Dubois, "Kron's method and cell complexes for magnetomotive and electromotive forces," *Int. J. Appl. Math.*, vol. 44, no. 4, pp. 183–191, 2014.
[30] C. Cholachue, B. Ravelo, A. Simoens, and A. Fathallah, "Fast S-parameter TAN model of n-port lumped structures," *IEEE Access*, vol. 7, pp. 72505–72517, 2019.
[31] O. Maurice. (2019). *Proposal of a Method for Systematic Electrothermal Analysis HAL-02054761, Version 1*. [Online]. Available: https://hal.archives-ouvertes.fr/hal-02054761
[32] A. Thavlov and H. W. Bindner, "Thermal models for intelligent heating of buildings," in *Proc. Int. Conf. Appl. Energy (ICAE)*, Suzhou, China, Jul. 2012, pp. A10591–A106000.
[33] Y. S. Touloukian, "Thermophysical properties of matter—The TPRC data series—A comprehensive compilation of data," Purdue Univ., West Lafayette, IN, USA, Tech. Rep. AD A129113, 1974, vol. 10, pp. 1–661.
[34] F. El Fgaier, Z. Lafhaj, F. Brachelet, E. Antczak, and C. Chapiseau, "Thermal performance of unfired clay bricks used in construction in the north of france: Case study," *Case Stud. Construct. Mater.*, vol. 3, pp. 102–111, Dec. 2015.
[35] H. Johra and P. Heiselberg, "Influence of internal thermal mass on the indoor thermal dynamics and integration of phase change materials in furniture for building energy storage: A review," *Renew. Sustain. Energy Rev.*, vol. 69, pp. 19–32, Mar. 2017.
[36] G. Kron, *Tensor Analysis of Networks*. New York, NY, USA: GE Collection, 1939.

RIVO RANDRIATSIFERANA (Member, IEEE) received the Engineering degree in industrial computer science and electronic from the École Supérieure Polytechnique d'Antsiranana (ESPA), University of Antsiranana, Madagascar, in 2009, and the Ph.D. degree in networks and telecommunications from the University of Reunion, Reunion Island, France, in 2014. He is currently a Research Associate with the Energy, Electronic and Process Laboratory, Science and Technology Department, University of La Reunion. His research interests include wireless networks communication with emphasis on architecture and protocol while considering RF energy and networking parameters: low receiver sensitivity, energy routers, and residual energy, design, characterization, energy modelling, and analysis of passive wake-up circuit for wireless sensor networks. His current research directions include advanced application of the tensor analysis of the network in smart building and smart object communications.

LALA RAJAOARISOA received the M.Sc. and Ph.D. degrees in automatic and computer sciences from the University of Aix-Marseille, France, in 2005 and 2009, respectively. He is currently an Assistant Professor with the Institut Mines-Télécom Lille Douai. He is involved in research activities dedicated to the optimization of energy efficiency of building systems and the control and management of hydraulic systems, with more than 80 papers published in refereed journals and conferences. His research interests include the development of data-driven tools and methods for the observation and control of large-scale distributed systems, and the development of predictive models and controllers to assess system behavior and optimize its performance. His development includes the analysis of intrinsic properties, such as stability, observability, identifiability, and controllability. He regularly participates and contributes on several international projects (ANR, FUI, and INTERREG) and was the supervisor of more than of 15 Ph.D. students, postdocs, research engineers, and Master internships.

SAMUEL NGOHO graduated from ESIGELEC, Rouen, France, in 2012. He received the Ph.D. degree in the thematic of high frequency electronics, photonics, and systems from the XLIM Laboratory, University of Limoges, Limoges, France. His Ph.D. subject was based on the design and production of integrated optoelectronic components for high speed telecommunications systems. He worked as an Integration, Verification, Validation, and Qualification Engineer of RF/HF products and systems for civil and military applications. He is currently working as a System Engineer with THALES SIX, Gennevilliers, France. He is interested in the progress of microelectronics, in particular in the development of innovative functions integrated in microwave devices to meet the need for densification and evolution of spectra for future communications systems. He also takes part within research groups in the use of unfamiliar methods for resolving complex system as Kron's method.

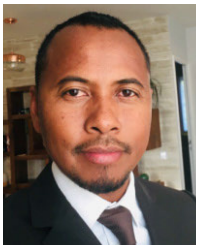

WENCESLAS RAHAJANDRAIBE (Member, IEEE) received the B.Sc. degree in electrical engineering from the University of Nice Sophia-Antipolis, France, in 1996, the M.Sc. degree (Hons.) in electrical engineering from the Department of Science, University of Montpellier, France, in 1998, and the Ph.D. degree in microelectronics from the University of Montpellier. In 1998, he joined the Microelectronics Department, Informatics, Robotics and Microelectronics Laboratory of Montpellier (LIRMM). In 2003, he joined the Microelectronic Department, Materials, Microelectronics and Nanoscience Laboratory of Provence (IM2NP), Marseille, France, where he was an Associate Professor. Since 2014, he has been a Professor with Aix-Marseille University, where he heads the Integrated Circuit Design Group, IM2NP Laboratory. He is currently a Full Professor with the University of Aix-Marseille. He is regularly involved to participate and to lead national and international research projects (ANR, H2020, and FP7 KIC-InnoEnergy). He directed and co-supervised 18 Ph.D. and 15 Master students. His research interests include AMS and RF circuit design from transistor to architectural level. His current research activity is focused on ultralow power circuit design for smart sensor interface and embedded electronic in bioelectronic and e-health applications, wireless systems, design technique, and architecture for multi-standard transceiver. He is author or coauthor of more than 150 papers published in refereed journals and conferences and holds 11 patents. He is an expert for the ANR, the French Agency for Research. He has served on program committees for the IEEE NEWCAS and ICECS. He has been and is a reviewer of contributions submitted to several IEEE conferences and journals, such as ISACS, NEWCAS, MWSCAS, ESSCIRC, ESSDERC, RFIC, the IEEE TRANSACTIONS ON CIRCUITS AND SYSTEMS I and II, and *Electronics Letters* (IET).

BLAISE RAVELO (Member, IEEE) is currently a University Full Professor with NUIST, Nanjing, China. His research interests include multiphysics and electronics engineering. He is a pioneer of the negative group delay (NGD) concept about $t<0$ signal travelling physical space. His extraordinary concept is potentially useful for anticipating and prediction all kind of information. He was the Research Director of ten Ph.D. students (seven defended), postdocs, research engineers, and Master internships. He is also a Lecturer of circuit and system theory, STEM (science, technology, engineering, and maths), and applied physics. With U.S., Chinese, Indian, European, and African partners, he is actively involved and contributes on several international research projects (ANR, FUI, FP7, INTERREG, H2020, Euripides^2, and Eurostars). He is a member of IET *Electronics Letters* editorial board, as a Circuit and System Subject Editor. He has been a member of scientific technical committee of Advanced Electromagnetic Symposium (AES), since 2013. In 2020, his Google Scholar H-index is 21. He is a member of the research groups, including the IEEE, URSI, GDR Ondes, and Radio Society, and (co)authored of more than 270 scientific research papers in new technologies published in international conference and journals. He is regularly invited to review papers submitted for publication to international journals, including the IEEE TRANSACTIONS ON MICROWAVE THEORY AND TECHNIQUES, the IEEE TRANSACTIONS ON CIRCUITS AND SYSTEMS, the IEEE TRANSACTIONS ON ELECTROMAGNETIC COMPATIBILITY, the IEEE TRANSACTIONS ON INDUSTRIAL ELECTRONICS, IEEE ACCESS, IET CDS, and IET MAP, and books in Wiley and Intech Science.